

Optical polarization variations in the blazar PKS 1749+096

Makoto UEMURA¹, Ryosuke ITOH², Ioannis LIODAKIS³, Dmitry BLINOV^{3,4},
Masanori NAKAYAMA⁵, Longyin Xu⁵, Naoko SAWADA⁵, Hsiang-Yun Wu⁵
and Issei FUJISHIRO⁵

¹Hiroshima Astrophysical Science Center, Hiroshima University, Kagamiama 1-3-1,
Higashi-Hiroshima, 739-8526, Japan

²Department of Physics, Tokyo Institute of Technology, 2-12-1 Ohokayama, Meguro, Tokyo
152-8551, Japan

³Department of Physics and Institute for Theoretical and Computational Physics (ITCP),
University of Crete, 71003, Heraklion, Greece

⁴Astronomical Institute, St. Petersburg State University, Universitetsky pr. 28, Petrodvorets,
198504 St. Petersburg, Russia

⁵Department of Information and Computer Science, Keio University 3-14-1 Hiyoshi,
Kohoku-ku, Yokohama 223-8522, Japan

*E-mail: uemuram@hiroshima-u.ac.jp

Received ; Accepted

Abstract

We report on the variation in the optical polarization of the blazar PKS 1749+096 observed in 2008–2015. The degree of polarization (PD) tends to increase in short flares having a time-scale of a few days. The object favors a polarization angle (PA) of 40°–50° at the flare maxima, which is close to the position angle of the jet (20°–40°). Three clear polarization rotations were detected in the negative PA direction associated with flares. In addition, a rapid and large decrease in the PA was observed in the other two flares, while another two flares showed no large PA variation. The light curve maxima of the flares possibly tend to lag behind the PD maxima and color-index minima. The PA became –50° to –20° in the decay phase of active states, which is almost perpendicular to the jet position angle. We propose a scenario to explain these observational features, where transverse shocks propagate along curved trajectories. The favored PA at the flare maxima suggests that the observed variations were governed by the variations in the Doppler factor, δ . Based on this scenario, the minimum viewing angle of the source, $\theta_{\min} = 4.8^\circ$ – 6.6° , and the location of the source, $\Delta r \gtrsim 0.1$ pc, from the central black hole were estimated. In addition, the acceleration of electrons by the shock and synchrotron cooling would have a time-scale similar to that of the change in δ . The combined effect of the variation in δ and acceleration/cooling of electrons is probably responsible for the observed diversity of the polarization variations in the flares.

Key words: BL Lacertae objects: individual (PKS 1749+096) — galaxies: jets — galaxies: active — polarization

1 Introduction

Blazars are a sub-class of active galactic nuclei (AGN) that can be observed if the jet axis is directed toward the Earth. The emission from the jet is enhanced because of the Doppler beaming effect. The relativistic beaming is also responsible for violent variability, which is commonly observed in blazars (Blandford, Rees 1978). These features make blazars excellent targets to understand the physics of jets.

The radio–X-ray emission from blazars is dominated by the synchrotron emission from jets, although the other components, such as the broad line region and host galaxy can contaminate the emission. Flat-spectrum radio quasars (FSRQs) are blazars that have emission lines originated from AGN in the optical spectrum (equivalent width, $\text{EW} \gtrsim 5 \text{ \AA}$). BL Lac objects (BL Lacs), on the other hand, exhibit no or only weak emission lines. BL Lacs are further divided into sub-classes depending on the peak frequency of the synchrotron emission, i.e., low-, intermediate-, and high-peaked BL Lacs (LBLs, IBLs, and HBLs, respectively; Abdo et al. 2010a).

In FSRQs and LBLs, the synchrotron emission is optically thin in the optical and near-infrared (NIR) regime. As a result, high and variable polarization can be observed in these wavebands. Recently, the rotation, or swing, of the polarization position angle (PA) has received attention as a promising probe for jet and magnetic field structures (Marscher et al. 2008; Abdo et al. 2010b; Marscher et al. 2010). However, it has been noted that interpretation of the observed variation in polarization is not straightforward because apparent PA rotations can also be made by non-deterministic random variations of polarization (Ikejiri et al. 2011; Blinov et al. 2015; Larionov et al. 2016). The observed polarization possibly consists of multiple components, which also complicates the interpretation (Uemura et al. 2010; Ikejiri et al. 2011). Therefore, to extract meaningful information, the polarization data must be carefully analyzed not only with respect to the time-series of the degree of polarization (PD) and PA , but also with respect to the movement in the Stokes QU plane, on an object-by-object basis. In addition, the polarization variation should be interpreted with other types of data, such as variations in the total flux, color, and multi-wavelength data.

PKS 1749+096 (also known as OT 081 and 4C +09.57) is a BL Lac object at $z = 0.322$ (Stickel et al. 1988), of which the optical polarization behavior is poorly known. According to Ghisellini et al. (2011), the spectral energy distribution (SED) of the object can be explained by a model with a magnetic field $B = 1.5 \text{ G}$, bulk Lorentz factor $\Gamma = 10$, and viewing angle $\theta = 3^\circ$. The SED suggests an LBL nature, while the strong emission line ($\text{EW} = 12.5 \text{ \AA}$) implies that it may be a transition object between an FSRQ and BL Lac (Ghisellini et al. 2011). Lu et al. (2012) reported a detailed study of very-long baseline interferometry (VLBI) observations of the object. The position angles

of the radio knots range between 20° – 40° in the downstream region of the jet, while they exist in a wider range in the upstream region. From the motion of the radio knots, a minimum Lorentz factor of 10.2 was estimated. Hovatta et al. (2009) and Liodakis et al. (2017) estimated Γ and θ of the variable component to be $(\Gamma, \theta) = (7.5, 3.8^\circ)$ and $(7.8, 2.3^\circ)$, respectively, based on the characteristics of radio flares of the object. According to Itoh et al. (2016), γ -ray flares of the object were detected by the Large Area Telescope on the *Fermi Gamma-ray Space Telescope* spacecraft (LAT/Fermi), while it is a faint source at quiescence. Optical flares are associated with the γ -ray flares.

Early historical observations show that the optical PD of PKS 1749+096 varied between a few and $\sim 10\%$, which is very typical for blazars (Kinman 1976; Wills et al. 1980; Impey et al. 1984). Brindle et al. (1986) detected a violent polarization flare from $PD \sim 10\%$ to 30% within a period of four days. Ikejiri et al. (2011) performed the first intense photo-polarimetric monitoring of this object, and obtained 78 data points over two years. The data revealed that a polarization rotation event was associated with a flare. Recently, Blinov et al. (2016b) and Blinov et al. (2016a) also reported optical polarization rotations of this object. These observations suggest that PKS 1749+096 is a good source to study the polarization rotation in blazars. Ikejiri et al. (2011) reported that the correlation between the total flux and the PD is weak, although they did not consider potential time-lags between these parameters.

In this paper, we present the first detailed study of the variation in the optical polarization of PKS 1749+096 based on the data obtained by the Kanata 1.5 m telescope and the RoboPol polarimeter attached to the 1.3-m telescope of Skinakas observatory (Ikejiri et al. 2011; Itoh et al. 2016; King et al. 2014). The data and reduction procedure are described in section 2 and the observational results are reported in section 3. We discuss the implications from the results in section 4, and summarize our findings in section 5.

2 Observations

Optical and NIR photo-polarimetric observations were performed with the 1.5-m Kanata telescope in Higashi-Hiroshima observatory and 1.3-m telescope in Skinakas observatory.

The data obtained with Kanata are those published in Itoh et al. (2016). Observations and data-reduction are fully described in Itoh et al. (2016). Here, we give a brief overview of the data shown in this paper. The observations were performed with the TRISPEC and HOWPol instruments (Watanabe et al. 2005; Kawabata et al. 2008). Both instruments have a polarimeter mode that uses a rotating half-wave plate and Wollaston prism. A set of linear polarization parameters is obtained with four consecutive exposures at half-wave plate position angles of 0.0° , 45.0° , 22.5° , and 67.5° . The exposure time

of each frame was typically 200 s, depending on the sky conditions. V and J band data were obtained simultaneously with TRISPEC, and V band data with HOWPol from 2008 to 2010. Data-reduction involved a standard photometry procedure; after dark-subtracted and flat-fielded images were produced, aperture photometry was performed with the APPHOT package in PyRAF and differential photometry with a comparison star taken in the same frame. Fractional Stokes parameters, $q = Q/I$ and $u = U/I$, were obtained from the photometry of ordinary and extra-ordinary light images. PD and PA were calculated from q and u : $PD = \sqrt{q^2 + u^2}$ and $PA = 0.5 \arctan(u/q)$.

The data in the Skinakas observatory were obtained with the RoboPol polarimeter attached to the 1.3m telescope. The polarimeter was specifically designed for the blazar monitoring program. It has no moving parts besides the filter wheel in order to avoid unmeasurable errors caused by sky changes between measurements and the non-uniform transmission of a rotating optical element (King et al. 2014). The data were taken in the R band from 2014 and 2015. In this paper, we use re-analyzed data which were reported in Blinov et al. (2016b) and Blinov et al. (2016a).

Sixty seven sets of four variables were used in this work, i.e., V band magnitude, Q/I , U/I (or PD , PA), and the J band magnitude from MJD 54666 to 55085 obtained with TRISPEC, 5 sets of three variables, V band magnitude, Q/I , and U/I from MJD 55274 to 55444 with HOWPol, and 46 sets of R band magnitude, Q/I , and U/I from MJD 56775 to 57285 with RoboPol. The V and R bands are so close in the wavelength domain that the difference of variability features is not discussed in this paper.

It is difficult to identify and extract interesting patterns from such multi-dimensional time-series data. To overcome this difficulty, a visualization tool was developed for the blazar polarization, which is called TimeTubes (Uemura et al. 2016). This tool enables identification of the variations in the magnitude, color index, Q/I , U/I , and their respective errors in one view, and facilitates noteworthy pattern recognition. We emphasize that the most important finding in this work was not from standard scatter plots, but from the use of TimeTubes. We show several examples of the TimeTubes view of the data from PKS 1749+096 in Appendix 1.

3 Results

Figure 1 shows the light curves, PD and PA variations of the object observed by Kanata in 2008 (left), 2009 (middle), and 2010 (right). The data taken within the same period of time are indicated by the same colors in each year. Table 1 lists the features of the flares described below.

The object experienced historically bright states in 2008. It was also in the brightest state in gamma-rays (Itoh et al. 2016).

The light curve in 2008 can be described with the two active states around MJD 54660–54720 and 54720–54790. In addition, short flares are superimposed on those active states. Four short flares were identified, flares A, B, C, and D, as indicated in the light curve. The observed peak times of the V -band magnitude for each flare, T_{\max} , are listed in Table 1.

Figure 2 shows the distribution and trajectories of $(Q/I, U/I)$ in 2008–2010. The upper-left panel shows the trajectory during flare A, indicated by the red points and gray lines. The trajectory indicates an apparent clockwise rotation in the PA . The large red symbol is the data at T_{\max} of the flare. The data for flares B, C, and D are also shown with each flare maximum emphasized by large symbols in figure 2. As can be seen from those large symbols, the maxima of flares A, C, and D have similar PAs around 40° – 50° . The PAs at T_{\max} , called as PA_{peak} , are listed in Table 1. In contrast to flare A, no hint of polarization rotation was seen in our available data of flares C and D, while those flares were not well observed. In the left panels of Figure 1, the blue and cyan symbols correspond to the data in the fading phase from the first and second active states. We call them decays A and B. Figure 2 shows that the polarization of these decay phases favors negative U/I .

The middle panels in Figure 1 show the data from 2009. Flare E was identified, as indicated by the red symbols. The observed maximum of this flare has a PA close to that of flare C, as shown in Figure 2 and Table 1. Figure 2 shows that the PA changed dramatically during the flare. The direction of variation in PA is again negative, as in the case of flare A, while the number of data is insufficient to clearly define the polarization variation. After flare E, the object retained a faint state with a possible minor flare, as shown by the green symbols in the figures. Large negative U/I values were recorded during this phase, as observed in decay A.

The data from 2010 are shown in the right panels of Figure 1. Larionov et al. (2010) reported an optical flare of this object in this year; $R = 15.28$ mag on 17 Aug. 2010. Following this report, we began observations on 22 Aug. The object was the brightest on this night ($V = 14.70$ at 22.59 UT Aug), and then faded. Figure 1 shows the light curve of this flare. Two more measurements were obtained after the peak. While the $V - R$ color is unknown during this flare, the object was presumably brighter on 22 Aug. than that on 17 Aug. because LBL have a typical color of $V - R \sim 0.5$, which indicates $V \sim 15.7$ on 17 Aug. (Gaur et al. 2012). This converted magnitude is shown as the open blue circle in the light curve, which is called flare F here. The PA of the observed maximum of flare F is close to that of flare E. The object experienced a rapid and large decrease in the PA during the fading phase of this flare, as observed in flares A and E.

Figures 3 and 4 are the same as Figures 1 and 2, but for the data observed by RoboPol in 2014 and 2015. Blinov et al.

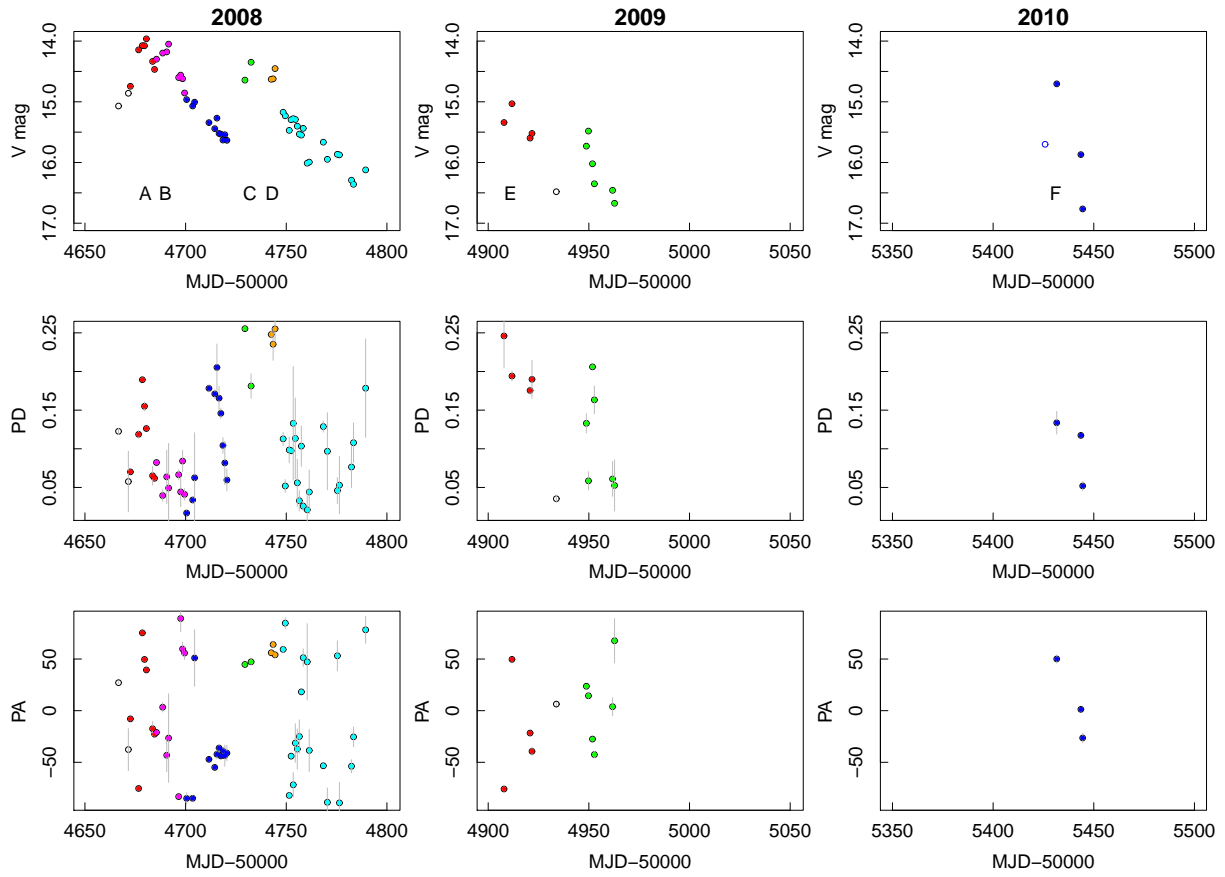


Fig. 1. V -band light curves (top panels), PD (middle panels), and PA variations (bottom panels) of PKS 1749+096 observed by Kanata. The left, middle, and right panels are those for the data obtained in 2008, 2009, and 2010, respectively. The data taken within the same period of time is represented by the same colors in each year. The six flares defined in the main text are indicated by A to F in the top panels. The open blue symbol in the light curve in 2010 is the converted data points in Larionov et al. (2010) (for more detail, see the text).

Table 1. Features of the flares.

Flare ID	T_{\max}^* (MJD)	ΔT_c^\dagger (day)	ΔT_{PD}^\ddagger (day)	PD_{\max}^\S (%)	PA_{peak}^\P (deg.)	dPA/dt^{\parallel} (deg. d $^{-1}$)
A	54680.52	3.86	2.00	18.9 ± 0.1	39.4 ± 0.2	-16.7 ± 0.4
B	54691.55	6.01	—	—	—	—
C	54732.52	3.06	3.06	25.5 ± 0.3	47.3 ± 2.7	—
D	54744.43	0.00	0.00	25.5 ± 1.7	54.1 ± 2.5	—
E	54911.81	3.95	3.95	24.6 ± 4.1	49.7 ± 1.1	-9.7 ± 0.8
F	55431.59	—	0.00	13.4 ± 1.5	50.1 ± 4.0	-5.1 ± 1.6
G	56887.83	—	3.96	24.0 ± 0.7	79.4 ± 1.0	-10.5^{**}
H	57213.88	—	0.00	11.7 ± 0.6	46.1 ± 1.5	$-9.0^{\dagger\dagger}$

* Times of the observed maxima in the total flux. \dagger Time differences of the observed minima in the $V - J$ color index from T_{\max} . The color is not available for flare F. \ddagger Time differences of the observed maxima in the PD from T_{\max} . \S Observed maximum values of the PD. \P PA at T_{\max} . These three features are not given in flare B, because no clear polarization flare was associated with it. \parallel Temporal gradient of the PA for flares in which large variations of PA were detected. **Blinov et al. (2016b). $\dagger\dagger$ Blinov et al. (2016a).

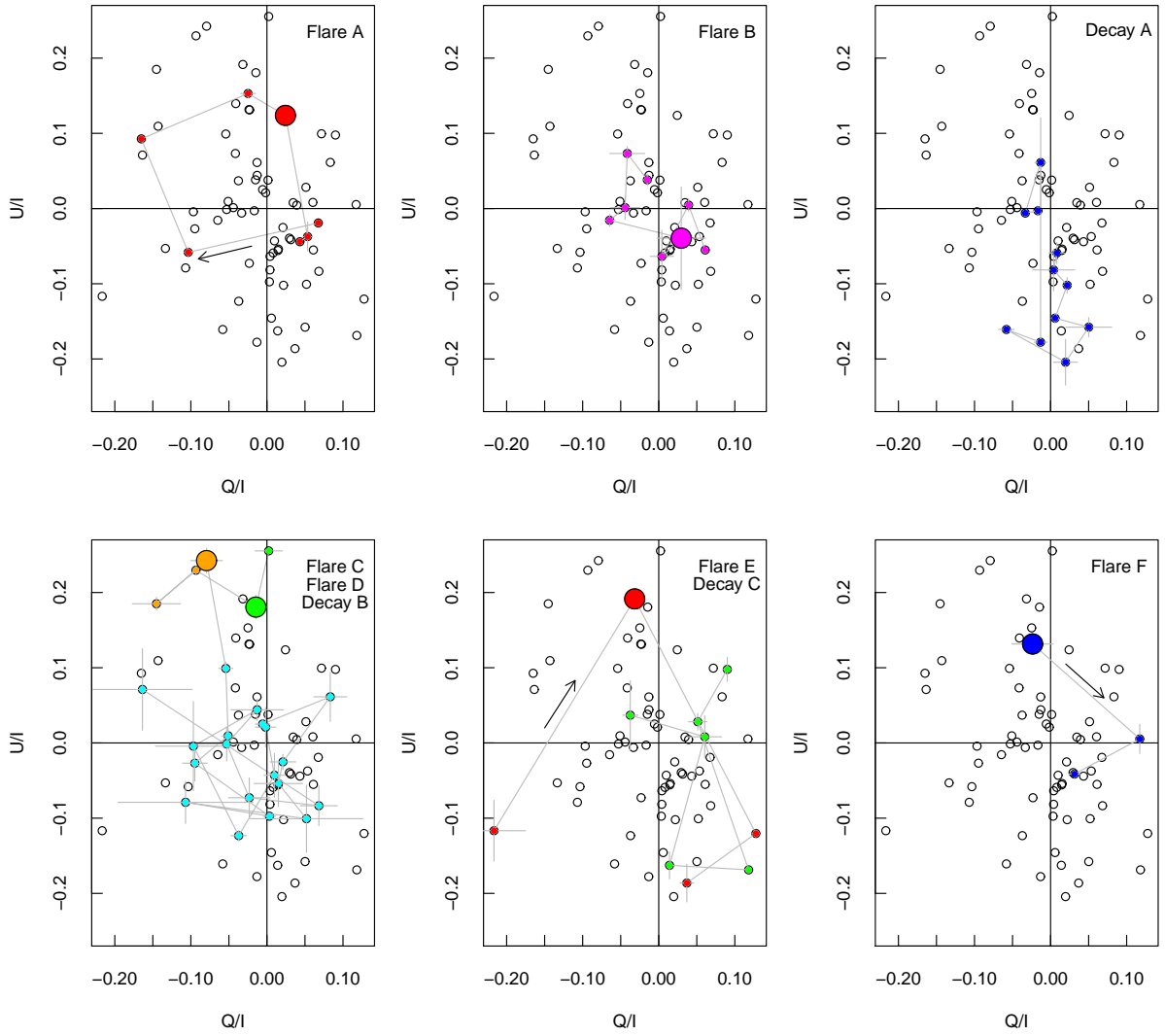


Fig. 2. The distribution and trajectories of $(Q/I, U/I)$ of PKS 1749+096 in 2008–2010. The flares and decay phases which are defined in the text and indicated in figure 1 are emphasized with the filled circles in each panel. All data points in 2008–2010 are indicated by the open circles. The data taken within the same period of time in figure 1 is represented by the same colors. The large symbols indicate the flare maxima. The moving directions are indicated by the arrows for flare A, E, and F.

(2016b) and Blinov et al. (2016a) reported two polarization rotation events in this period of time.

The first event was observed in MJD 56860–56900 with a rotation rate of $dPA/dt = -10.5 \text{ deg d}^{-1}$, and a PA amplitude of 335.1° (Blinov et al. 2016b). The period of this event is indicated by the red points in the left panels of Figure 3 and upper panels of Figure 4. The event was associated with an optical flare, of which the maximum occurred at when $PA = 79.4 \pm 1.0^\circ$. We call this flare as flare G. The characteristics of the trajectory on the $(Q/I, U/I)$ plane are analogous to those of flares A, E, and F, that is, a clockwise rotation with high PD , as shown in figure 4. Besides the flare, the object favors negative U/I . The object was in the faintest state during our observations before the flare.

The second event was observed in MJD 57210–57240 with a rotation rate of $dPA/dt = -9.0 \text{ deg d}^{-1}$, and a PA amplitude of 224.5° (Blinov et al. 2016a). The period is indicated by the red points in the right panels of Figure 3 and lower panels of Figure 4. This event was unique in terms of both the light curve and polarization variation. The object kept a level slightly brighter than the quiescence, and favors an area of positive Q/I and U/I throughout 2015. These features are probably due to the emergence of a new emitting component having the polarization of positive Q/I and U/I . A possible short flare, which we call flare H, was observed at the onset of the polarization rotation when $PA = 46.1 \pm 1.5^\circ$. PDs were small during the polarization rotation, except for the short flare.

Figure 5 shows the PD (filled circles) and $V - J$ (open cir-

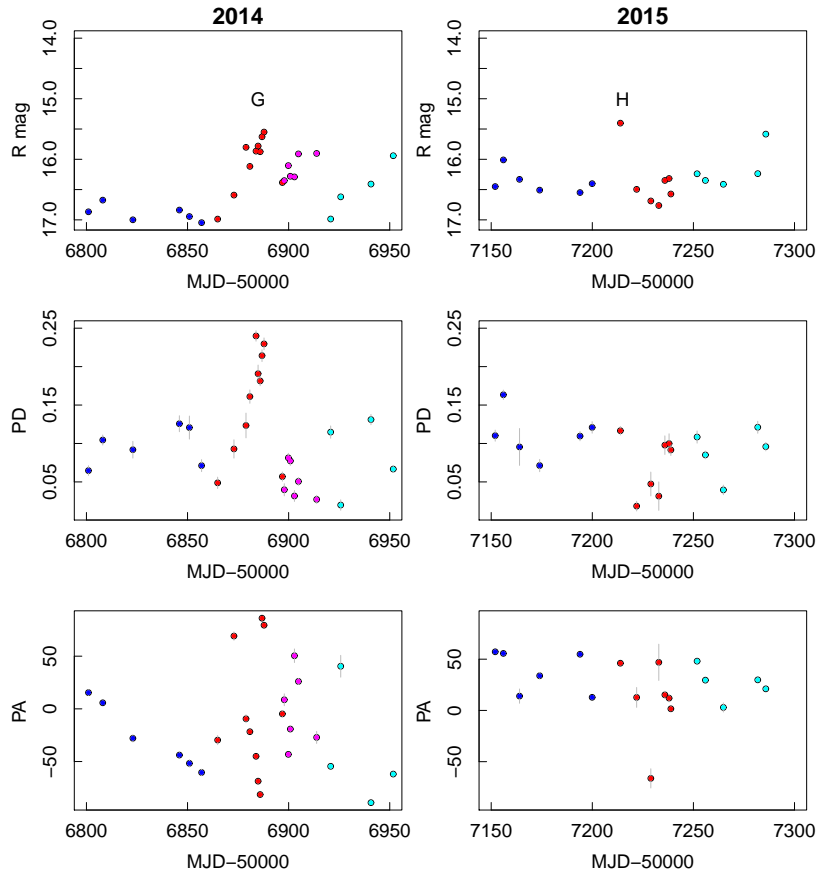


Fig. 3. R -band light curves (top panels), PD (middle panels), and PA variations (bottom panels) of PKS 1749+096 observed by RoboPol. The left and right panels are those for the data obtained in 2014 and 2015, respectively. The scales and symbols are the same as those in Figure 1.

cles) variations of flares A, B, C, E, and G. The vertical dashed lines indicate T_{\max} of each flare. PD flares were associated with all flares, except for flare B, in which the PD remained low throughout the flare. Flare A was well observed in both the rising and decaying phases, which suggests a clear time-lag of T_{\max} against the PD maximum. Similarly, the observed PD maximum precedes T_{\max} in flares C and E. In flare G, the observed maximum of PD precedes T_{\max} by 4d. However, this PD peak is possibly not associated with the flare maximum because PD again increased toward T_{\max} . The time lags of T_{\max} against the observed peaks of $V - J$ (ΔT_c) and PD (ΔT_{PD}) are listed in Table 1. It should be noted that the number of data except for flare A is insufficient to make firm conclusions about the general trend of the time-lag. The lacks of time-lags in flares D, F, and H are mainly due to poorly-covered observations. In addition, those observed time-lags listed in Table 1 possibly have large uncertainties because they are obtained from observations with a typical cadence of a few days and some flares were poorly observed.

Figure 6 shows histograms of the PA . The histogram for all data in 2008–2010 (upper-left panel) suggests a concentration between $PA \sim 40^\circ - 50^\circ$. The other possible concentration can

be observed around $PA \sim -50^\circ$ to -20° . The upper-right panel of Figure 6 shows the PA distribution for the 2008–2010 data with $PD > 0.10$. The non-uniformity of the PA distribution is emphasized for the data with a high PD . The concentration of $PA \sim 40^\circ - 50^\circ$ originates from the data around the flare maxima. The other concentration of $PA \sim -50^\circ$ to -20° is due to the fading phases from the active states. It is noteworthy that the difference between those two favored PAs is $\sim 90^\circ$.

The lower panels of Figure 6 are the data from 2014 and 2015. The distribution of the all PA data (left) has a possible spike feature around $PA \sim 20^\circ - 30^\circ$. This is due to the data from 2015 which concentrates in the area of $Q/I > 0$ and $U/I > 0$. The PA distribution of $PD > 0.10$ (right) exhibits features similar to that in 2008–2010, that is, a concentration of $PA \sim 40^\circ - 50^\circ$.

4 Discussion

4.1 Transverse shock scenario for the short flares

The polarization variations and rotations associated with the short flares have common features, as shown in the previous section. First, their values of dPA/dt are of the same order

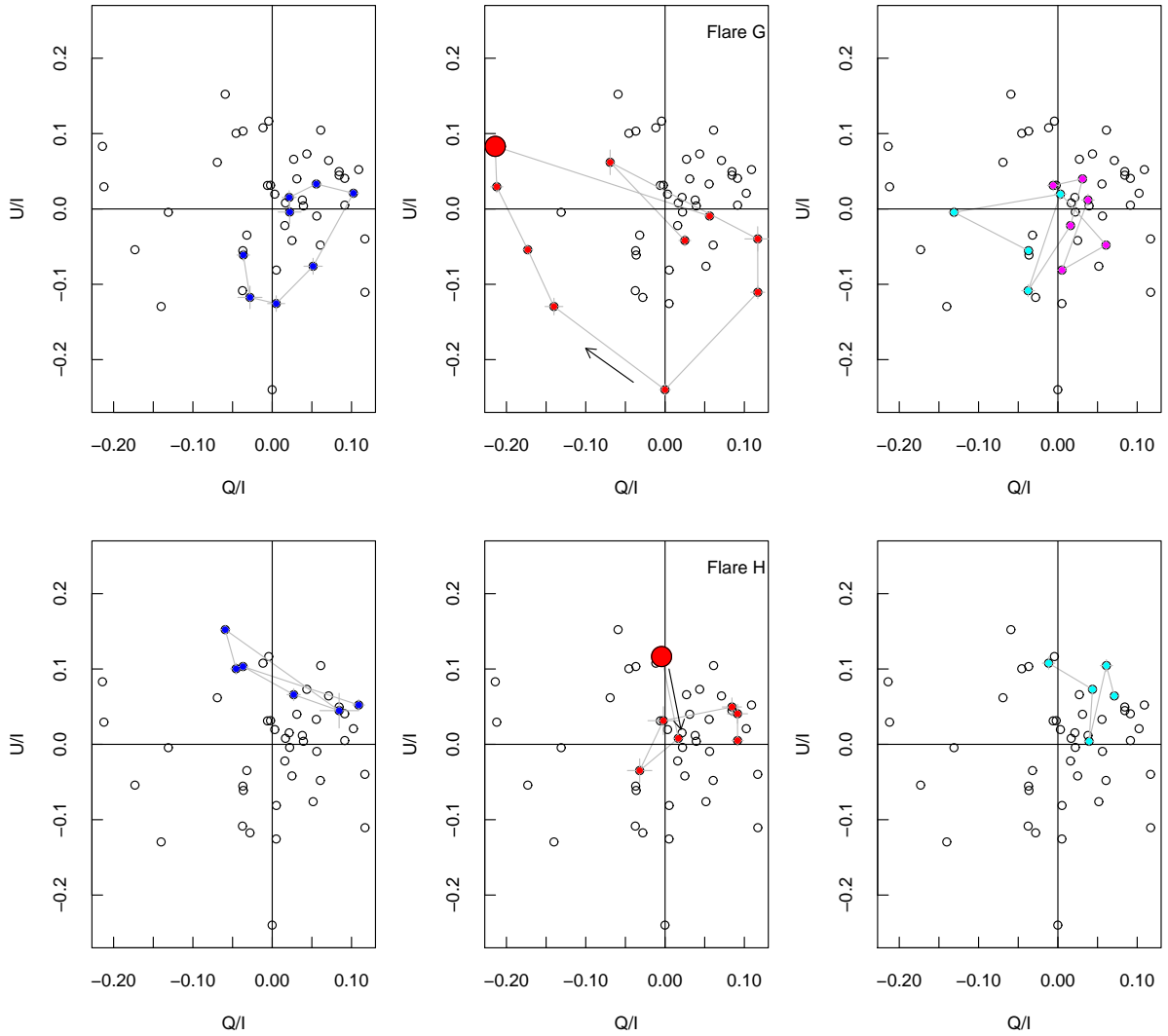


Fig. 4. The distribution and trajectories of $(Q/I, U/I)$ of PKS 1749+096 in 2014 and 2015. The scales and symbols are the same as those in Figure 2.

of magnitude as those shown in Table 1. Second, all detected rotations have negative dPA/dt . If the rotations are made by random variations, then the probability that five rotations are always in the negative direction is low at $0.5^5 \sim 0.03$. Finally, among 8 flares, six flares (A, C, D, E, F, and H) exhibit similar PA_{peak} . The PA_{peak} of Flare G ($\sim 79^\circ$) significantly deviates from those of the other flares. However, as noted by Blinov et al. (2016b), the object was not observed for 9.1 d after the observed maximum. During this period, the PA decreased from 79.4° to -4.8° . Therefore, the flare maximum could have a similar PA to those of our observations (40° – 50°) if the real maximum was between this period. These common features suggest that the polarization rotation events and flares have a common mechanism. We discuss it in this subsection.

We first focus on the fact that the object favors a narrow range of PA_{peak} . This feature suggests that the flares are

mainly caused by a geometrical effect. Here, we consider flaring sources that propagate along curved trajectories. In the case of the compact emission source, the observed flux $F(t)$, can be expressed as:

$$F(t) = F_0 \nu^{-\alpha} \delta^{(3+\alpha)}, \quad (1)$$

where F_0 and α are the flux in the co-moving frame of the jet and the spectral index, respectively (Dermer, Menon 2009). δ is the Doppler factor, which changes with time because the angle between the velocity vector of the source and the line-of-sight is a function of time. The flare maxima are observed at T_{max} when the viewing angle reaches the minimum at θ_{min} and δ is at maximum. A clear polarization swing (flare A) and two large PA variations around T_{max} (flares E and F) were detected. These PA variations are also expected in this scenario because the direction of the magnetic field can change

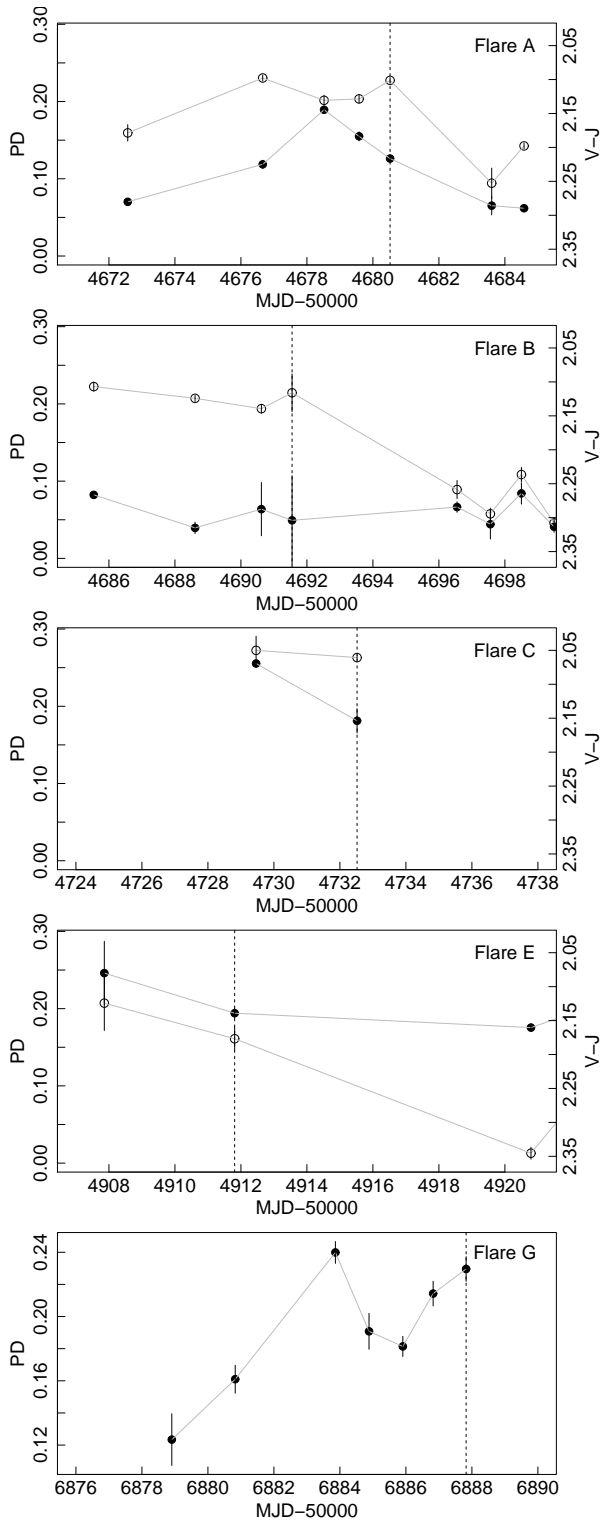


Fig. 5. PD and $V - J$ color variations of flares A, B, C, E, and G. The filled and open circles indicate PD and $V - J$, respectively. The observed maxima of each flare in the total flux are indicated by the dashed vertical lines. The $V - J$ data is not available for flare G.

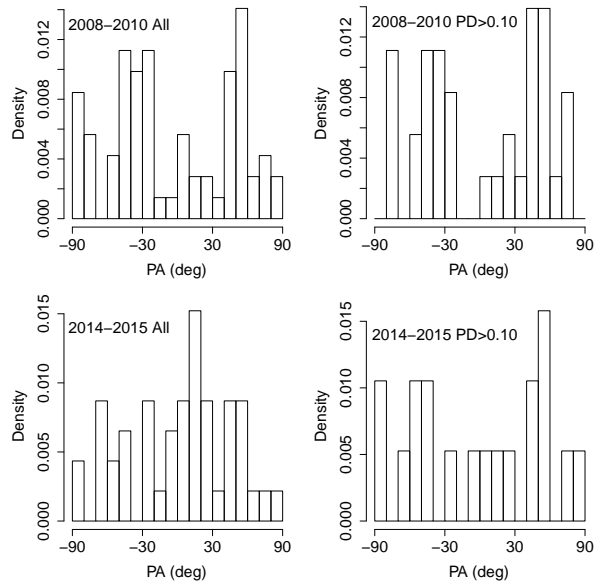


Fig. 6. Histograms of the PA for all data between 2008 and 2010 (upper-left panel), those for $PD > 0.10$ (upper-right panel), all data of 2014 and 2015 (lower-left), and those for $PD > 0.10$ (lower-right panel).

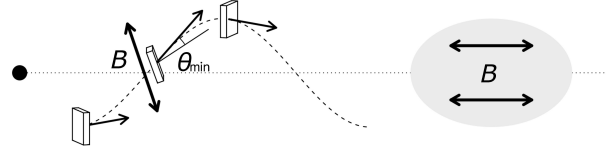


Fig. 7. Schematic view of the emitting region and magnetic field in the jet.

with the propagation of the source along with the curved trajectory (Bjornsson 1982; Konigl, Choudhuri 1985; Nalewajko 2010; Lyutikov, Kravchenko 2017).

The VLBI observations reported in Lu et al. (2012) show that the position angle of the jet is $20^\circ - 40^\circ$ in the downstream region, approximately 10 pc from the core, while the PA of the radio knots takes a wide range of values ($-20^\circ - 50^\circ$) in the upstream region. Our observation shows that the PA of T_{\max} is concentrated between $40^\circ - 50^\circ$, which is close to the jet position angle. This implies that the magnetic field in the flaring source is almost perpendicular to the jet direction at T_{\max} . Such a condition can be explained with the ordered magnetic field in a plasma compressed by a transverse shock (Marscher, Gear 1985; Hughes et al. 1985). Hagen-Thorn et al. (2008) proposed a similar scenario for the optical flare of the blazar AO 0235+164 to explain its PA close to the jet direction.

We note that all dPA/dt detected in flares A, E, F, G, and H are negative. This implies that the curved trajectory is governed by a fixed structure in the jet, and is time independent, at least on a time-scale of years. The helical magnetic field is a

candidate for such a structure, while the bending of the entire jet is also possible if the bending structure is time independent. Gabuzda et al. (2008) estimated the helicity of the magnetic field in AGN jets based on the observed rotation measure gradient and sign of parsec-scale circular polarization. They reported that PKS 1749+096 exhibits a right-handed helical magnetic field with an inward poloidal component which corresponds to the south magnetic poles. The helicity is consistent with the sign of dPA/dt that we observed if the emitting regions propagate along with the helical field to the downstream region of the jet.

Figure 7 illustrates a schematic view of this scenario. This is supported by the possible time-lag between the PD maxima and T_{\max} , as shown in Table 1 and Figure 5. The polarization variation of compressed plasma in a transverse shock is predicted by several theoretical models (Bjornsson 1982; Konigl, Choudhuri 1985; Zhang et al. 2016). According to such models, the timing of the PD maximum can be different from T_{\max} . This is because the total flux reaches the maximum when the shocked plane is faced and the emission is only weakly polarized. On the other hand, the PD reaches the maximum when the shocked region is observed with a larger viewing angle and the polarization is maximized. These polarization behavior can also be expected in the models that only consider the geometrical effect without compressed plasma (Nalewajko 2010; Lyutikov, Kravchenko 2017).

Nalewajko (2010) discusses the polarization variation of emitting blobs propagating on curved trajectories. In the model, the emitting blobs pass through the trajectories with a constant curvature radius R . The flare maximum is observed when the viewing angle becomes minimum at θ_{\min} . Then, the maximum value of dPA/dt and ΔT_{PD} are provided as function of R and θ_{\min} , as follows:

$$\frac{dPA}{dt}_{\max} = \frac{\Omega}{(1 - \beta_{blob} \cos \theta_{\min}) \sin \theta_{\min}}, \quad (2)$$

$$\Delta T_{PD} = \frac{1}{\Omega} \left[\arccos \left(\frac{\beta_{jet}}{\cos \theta_{\min}} \right) - \beta_{blob} \sqrt{\cos^2 \theta_{\min} - \beta_{jet}^2} \right] \quad (3)$$

where $\Omega = \beta_{blob} c/R$ is the angular velocity of the blob, and β_{blob} and β_{jet} are the ratios of the blob and jet velocities to the speed of light. As in Nalewajko (2010), we assume the blob and jet speeds are the same: $\beta = \beta_{blob} = \beta_{jet}$. β is given by the Lorentz factor Γ , of the blob and jet: $\beta = v/c = \sqrt{1 - \Gamma^{-2}}$. This model is applied to our observations of flare A, which gives $dPA/dt = -16.7 \pm 0.4 \text{ deg d}^{-1}$ and $\Delta T_{PD} = 2.00 \pm 1.00 \text{ d}$. Here, the uncertainty of ΔT_{PD} is roughly estimated to be 1.00 d based on the observation interval. Lu et al. (2012) reports the minimum Lorentz factor of this object to be $\Gamma = 10.2$ from the VLBI observations. Based on the characteristics of radio flares, Hovatta et al. (2009) and Liodakis et al. (2017) reports $\Gamma = 7.5$ and 7.8, respectively. For $\Gamma = 7.5\text{--}10.2$, the data of flare A and Equations (2) and (3) provide $R = 1.6\text{--}4.1 \text{ pc}$ and $\theta_{\min} = 4.8^\circ\text{--}$

6.6° . In Nalewajko (2010), the distance covered by the blob between the PD maxima and T_{\max} is given as a function of R and θ_{\min} : $\Delta r_{blob} = R \times \arccos(\beta_{jet}/\cos \theta_{\min}) = 0.1\text{--}0.2 \text{ pc}$.

Savolainen et al. (2010) reported that the viewing angle θ , of blazars that are not detected in γ -rays by LAT/Fermi ranges from 0° to 10° with a few exceptions having larger θ , and have a mean value of 4.4° . As mentioned in section 1, PKS 1749+096 is a faint γ -ray source at quiescence. According to Itoh et al. (2016), it is just around the 3-sigma detection limit in seven-day bins. The estimated θ_{\min} for flare A is a typical one for non-LAT-detected blazars, and close to that estimated in Savolainen et al. (2010) for PKS 1749+096 (4.2°). The estimated Δr_{blob} gives a lower limit of the distance from the central black hole. The location of the flaring source at $\gtrsim 0.1 \text{ pc}$ is consistent with the standard picture of blazars, in which the optical emitting sources are located in a sub-parsec region. Thus, the proposed scenario can explain the time-lag between the flare and rotation within the current understanding of blazars.

A problem is that the theoretical models generally provide two PD maxima both before and after T_{\max} . This is because they assume that the observed variation is only caused by the variation in δ . As a result, the PD variation is symmetric with respect to T_{\max} when symmetric trajectories on the position of θ_{\min} are considered. The PD peaks were detected before T_{\max} in three flares (flare A, C, E, and possibly G, as shown in Table 1), while no sign of the PD peak after T_{\max} was observed in 6 flares. It is possible that the second PD peaks were overlooked. Flares A, E, and G were not observed for a few days after T_{\max} , when the other PD peak may have been present. However, this idea is not favored by the data, because there is no observation bias to detect the first PD maximum more frequently than the second PD maximum.

Alternatively, the lack of the second PD maximum may be explained if the flaring sources rapidly decreased their flux density just after T_{\max} . That is, we consider the temporal variation in F_0 in Equation (1). Ghisellini et al. (2011) reported the SED of PKS 1749+096, which suggests that the optical waveband corresponds to the high frequency edge of the synchrotron emission. The optical emission thus originates from the electrons with the maximum energy. Therefore, it is possible that the decay of the flare is governed by the synchrotron cooling.

The synchrotron cooling time-scale of an electron in a homogeneous magnetic field in the observer's frame t_c , can be estimated as follows:

$$t_c = (\delta)^{-1} 5 \times 10^{11} (1+z)^{1/2} B^{-3/2} [\text{G}] (\nu_{\text{obs}} [\text{Hz}] / \delta)^{-1/2} [\text{s}] \quad (4)$$

where B and ν_{obs} are the magnetic field and observation frequency (Tucker 1975). Based on the SED analysis, Ghisellini et al. (2011) reported $B = 1.5 \text{ G}$ for PKS 1749+096. Lu et al. (2012) estimated $\delta = 10.2\text{--}20.4$ from VLBI observations. Using these values, we estimated $t_c = 0.03\text{--}0.05 \text{ d}$. The estimation of

t_c is highly dependent on B , as evident from Equation (4). If we use $B = 0.15$ G, which is one order of magnitude lower than that proposed, but still acceptable for blazars (Ghisellini et al. 2011), t_c is estimated to be 1.08–1.53 d. These estimates suggest that the electrons accelerated by the shock possibly lose the energy by synchrotron cooling in a time-scale less than days. Therefore, the second PD maximum may be missed if significant cooling starts between the first PD maximum and T_{\max} .

The observed color variations also imply that we observed the acceleration and cooling processes by the shock during the flares. The color of the object was bluest 3–6 d before T_{\max} for flares A, B, C, and E, as shown in Table 1. These color variations are sometimes referred to as spectral hysteresis, i.e., a loop track in a spectral hardness–intensity diagram (Takahashi et al. 1996; Kataoka et al. 2000; Ikejiri et al. 2011). This is explained by the scenario that high energy electrons decay by rapid cooling, which results in growth of the flaring synchrotron source with the decreasing peak frequency. Böttcher, Dermer (2010) calculated the spectral variations of shocks in colliding plasma shells, and reproduced the spectral hysteresis.

Böttcher, Dermer (2010) also simulated the optical light curves. The light curve consists of three phases: i) a rapid rise by the onset of electron acceleration, ii) a gradual rise in which the shock locates within the colliding shells, and iii) a rapid decay by synchrotron cooling. We propose that the flares in PKS 1749+096 were caused by such internal shocks in conjunction with the variations in δ , which have a timescale analogous to that of the shock acceleration/cooling. A similar model was proposed by Larionov et al. (2013) for the flares of S5 0716+714 in which polarization rotations were associated. In our scenario, the observed polarization variation was dependent on the timing for the start of acceleration/cooling relative to the time of θ_{\min} . A PA swing would only be observed when the shock acceleration starts moderately before the source reaches the point of θ_{\min} . No flare would be observed if the cooling phase starts much earlier before the point of θ_{\min} or if the acceleration phase starts after it because δ is small. When a flare starts around the point of θ_{\min} , we could observe the flare without an apparent polarization swing because δ decreased after θ_{\min} . Flares C and D, in which no polarization swing was detected, and Flare G, in which PD is low during the rotation event, despite having similar PAs, may be examples of such cases. Thus, the combined effect of the variation in δ and acceleration/cooling of electrons may be responsible for the observed diversity of the polarization variations in the flares.

4.2 Polarization features of the decay phase

The object favors PAs between -50° and -20° during the decay phase from the active states, as mentioned in section 3. This PA range is $\sim 90^\circ$ different from the PA of the short flares at

maximum. In contrast to the magnetic field almost perpendicular to the jet axis for the short flare maxima, the magnetic field is expected to be parallel to the jet axis during the decay phase, as illustrated in Figure 7. The PD increased in the early decay stage, and then decreased in the latter stage.

In the decay phase, the electrons accelerated by the shock propagated to the downstream region of the jet, and were significantly cooled. The magnetic field of the source was probably not aligned by the shock compression. Instead, the original field, which is parallel to the jet axis, would be dominant. The electrons that were not fully cooled down were continuously added to the downstream region throughout the active state, which may be responsible for the observed variations in the PAs and PDs during the decay phase. The quiescent data observed in 2014 (the blue symbols in figure 3) shows a PA concentration similar to the decay phase, possibly indicating a long life-time of this component.

5 Summary

Optical–NIR photo-polarimetric observations of PKS 1749+096 in 2008–2015 were performed. We identified eight short flares having a time-scale of a few days. The polarization features of the object are summarized as follows.

- The PD tends to increase during the short flares.
- The object favors $PA = 40^\circ$ – 50° at the flare maxima, which is close to the position angle of the radio jet.
- Three clear polarization rotations associated with the flares were detected. The other two flares also showed large PA variations during the flares.
- The PD maxima possibly precede the maxima of the total flux by 2–4 d.
- The object favors $PA = -50^\circ$ to -20° in the decay phases from the active states.

We propose a transverse shock scenario which propagates along curved trajectories. This scenario can explain the observed dPA/dt and time-lag between the PD and flare maxima with reasonable conditions for blazars. The shock accelerating/cooling time-scale may be comparable to that of the change in δ .

Acknowledgments

We would like to thank Gina Panopoulou for her thoughtful and detailed comments on this paper. This work was supported by a Kakenhi Grant-in-Aid (No. 25120007) from the Japan Society for the Promotion of Science (JSPS). The U. of Crete group acknowledges support by the “RoboPol project”, which is co-funded by the European Social Fund (ESF) and Greek National Resources, and by the European Commission Seventh Framework Programme (FP7) through grants PCIG10-GA-2011-304001 “JetPop” and PIRSES-GA-2012-31578 “EuroCal”. RoboPol is a collaboration involving the University of

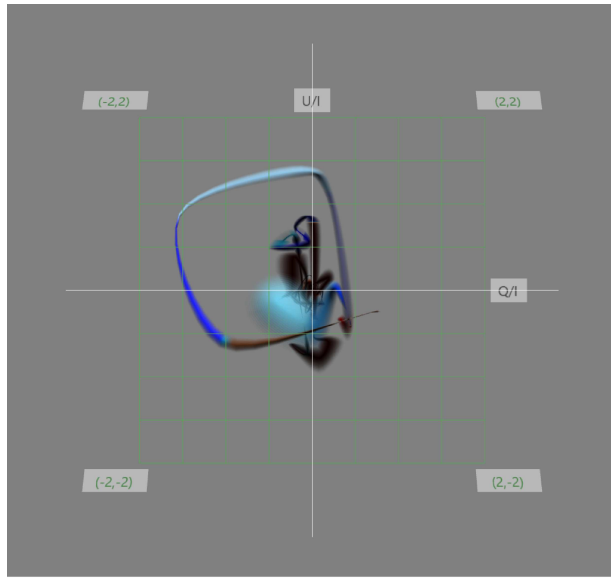


Fig. 8. TimeTubes view around flare A.

Crete, the Foundation of Research and Technology-Hellas, the California Institute of Technology, the Max-Planck Institute for Radio Astronomy, the Nicolaus Copernicus University, and the Inter-University Center for Astronomy and Astrophysics.

Appendix 1 TimeTubes views of the data from PKS 1749+096

Here, we introduce the TimeTubes visualization tool and an example of its use with PKS 1749+096 for future research using time-series polarization data similar to those presented in this paper. In TimeTubes, the trajectories of the object on the Stokes QU plane are expressed as tubes in 3D (Q , U , and time) space. The color phase and brightness of the tubes correspond to the observed flux and color index. The width of the tubes express the measurement errors of Q and U . TimeTubes thus enables the behavior of six variables (flux, color index, Q , U , and their errors) to be observed in one view.

Figure 8 shows a head-on view of TimeTubes for the data of PKS 1749+096. It shows the data around flare A, in which a clear polarization rotation was observed. This view indicates that the object was first faint and red, and then became bright and blue in association with the rotation. Figure 9 shows a side-view of TimeTubes around flares C and D. Here, the object experienced two flares, as indicated by the white color in the tube, at high U/I .

TimeTubes is available at the project site.¹

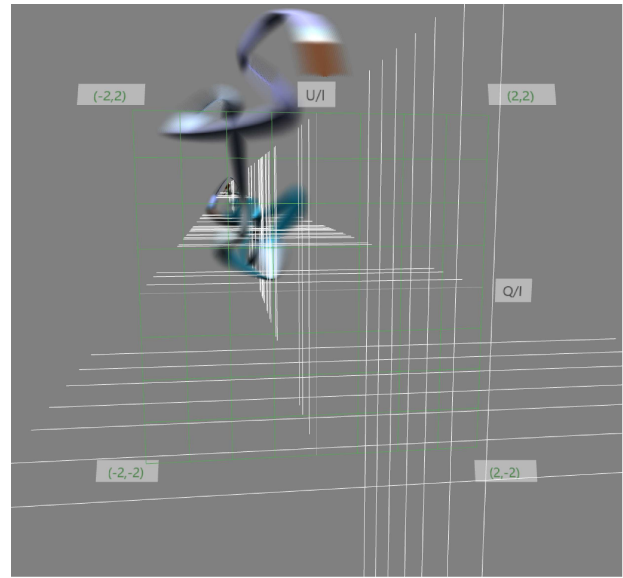


Fig. 9. TimeTubes view around flares C and D.

References

- Abdo, A. A., Ackermann, M., Agudo, I., Ajello, M., Aller, H. D., Aller, M. F., Angelakis, E., Arkharov, A. A., et al. 2010a, ApJ, 716, 30
- Abdo, A. A., Ackermann, M., Ajello, M., Axelsson, M., Baldini, L., Ballet, J., Barbiellini, G., Bastieri, D., et al. 2010b, Nature, 463, 919
- Bjornsson, C.-I. 1982, ApJ, 260, 855
- Blandford, R. D. & Rees, M. J. 1978, in BL Lac Objects, ed. A. M. Wolfe (University of Pittsburgh Press), pp 328–341
- Blinov, D., Pavlidou, V., Papadakis, I., Kiehlmann, S., Liodakis, I., Panopoulou, G. V., Pearson, T. J., Angelakis, E., et al. 2016a, MNRAS, 462, 1775
- Blinov, D., Pavlidou, V., Papadakis, I., Kiehlmann, S., Panopoulou, G., Liodakis, I., King, O. G., Angelakis, E., et al. 2015, MNRAS, 453, 1669
- Blinov, D., Pavlidou, V., Papadakis, I. E., Hovatta, T., Pearson, T. J., Liodakis, I., Panopoulou, G. V., Angelakis, E., et al. 2016b, MNRAS, 457, 2252
- Böttcher, M. & Dermer, C. D. 2010, ApJ, 711, 445
- Brindle, C., Hough, J. H., Bailey, J. A., Axon, D. J., & Hyland, A. R. 1986, MNRAS, 221, 739
- Dermer, C. D. & Menon, G. 2009, High Energy Radiation from Black Holes: Gamma Rays, Cosmic Rays, and Neutrinos (Princeton University Press)
- Gabuzda, D. C., Vitrihchak, V. M., Mahmud, M., & O'Sullivan, S. P. 2008, MNRAS, 384, 1003
- Gaur, H., Gupta, A. C., Strigachev, A., Bachev, R., Semkov, E., Wiita, P. J., Peneva, S., Boeva, S., et al. 2012, MNRAS, 425, 3002
- Ghisellini, G., Tavecchio, F., Foschini, L., & Ghirlanda, G. 2011, MNRAS, 414, 2674
- Hagen-Thorn, V. A., Larionov, V. M., Jorstad, S. G., Arkharov, A. A., Hagen-Thorn, E. I., Efimova, N. V., Larionova, L. V., & Marscher, A. P. 2008, ApJ, 672, 40

¹ (<http://fj.ics.keio.ac.jp/index.php/projects/spm/>)

- Hovatta, T., Valtaoja, E., Tornikoski, M., & Lähteenmäki, A. 2009, *A&A*, 494, 527
- Hughes, P. A., Aller, H. D., & Aller, M. F. 1985, *ApJ*, 298, 301
- Ikejiri, Y., Uemura, M., Sasada, M., Ito, R., Yamanaka, M., Sakimoto, K., Arai, A., Fukazawa, Y., et al. 2011, *PASJ*, 63, 639
- Impey, C. D., Brand, P. W. J. L., Wolstencroft, R. D., & Williams, P. M. 1984, *MNRAS*, 209, 245
- Itoh, R., Nalewajko, K., Fukazawa, Y., Uemura, M., Tanaka, Y. T., Kawabata, K. S., Madejski, G. M., Schinzel, F. K., et al. 2016, *ApJ*, 833, 77
- Kataoka, J., Takahashi, T., Makino, F., Inoue, S., Madejski, G. M., Tashiro, M., Urry, C. M., & Kubo, H. 2000, *ApJ*, 528, 243
- Kawabata, K. S., Nagae, O., Chiyonobu, S., Tanaka, H., Nakaya, H., Suzuki, M., Kamata, Y., Miyazaki, S., et al. 2008, in *Ground-based and Airborne Instrumentation for Astronomy II* Vol. 7014 of Proc. SPIE(. SPIE), 70144L
- King, O. G., Blinov, D., Ramaprakash, A. N., Myserlis, I., Angelakis, E., Baloković, M., Feiler, R., Fuhrmann, L., et al. 2014, *MNRAS*, 442, 1706
- Kinman, T. D. 1976, *ApJ*, 205, 1
- Konigl, A. & Choudhuri, A. R. 1985, *ApJ*, 289, 188
- Larionov, V., Jorstad, S., Marscher, A., & Smith, P. 2016, *Galaxies*, 4, 43
- Larionov, V. M., Blinov, D. A., Borisova, E. V., & Markelova, A. V. 2010, *The Astronomer's Telegram*, 2799
- Larionov, V. M., Jorstad, S. G., Marscher, A. P., Morozova, D. A., Blinov, D. A., Hagen-Thorn, V. A., Konstantinova, T. S., Kopatskaya, E. N., et al. 2013, *ApJ*, 768, 40
- Liodakis, I., Marchili, N., Angelakis, E., Fuhrmann, L., Nestoras, I., Myserlis, I., Karamanavis, V., Krichbaum, T. P., et al. 2017, *MNRAS*, 466, 4625
- Lu, R.-S., Shen, Z.-Q., Krichbaum, T. P., Iguchi, S., Lee, S.-S., & Zensus, J. A. 2012, *A&A*, 544, A89
- Lyutikov, M. & Kravchenko, E. 2017, ArXiv e-prints
- Marscher, A. P. & Gear, W. K. 1985, *ApJ*, 298, 114
- Marscher, A. P., Jorstad, S. G., D'Arcangelo, F. D., Smith, P. S., Williams, G. G., Larionov, V. M., Oh, H., Olmstead, A. R., et al. 2008, *Nature*, 452, 966
- Marscher, A. P., Jorstad, S. G., Larionov, V. M., Aller, M. F., Aller, H. D., Lähteenmäki, A., Agudo, I., Smith, P. S., et al. 2010, *ApJL*, 710, L126
- Nalewajko, K. 2010, *International Journal of Modern Physics D*, 19, 701
- Savolainen, T., Homan, D. C., Hovatta, T., Kadler, M., Kovalev, Y. Y., Lister, M. L., Ros, E., & Zensus, J. A. 2010, *A&A*, 512, A24
- Stickel, M., Fried, J. W., & Kuehr, H. 1988, *A&A*, 191, L16
- Takahashi, T., Tashiro, M., Madejski, G., Kubo, H., Kamae, T., Kataoka, J., Kii, T., Makino, F., Makishima, K., & Yamasaki, N. 1996, *ApJL*, 470, L89
- Tucker, W. 1975, *Radiation processes in astrophysics* (Cambridge, Mass., MIT Press)
- Uemura, M., Itoh, R., Xu, L., Nakayama, M., Wu, H.-Y., Watanabe, K., Takahashi, S., & Fujishiro, I. 2016, *Galaxies*, 4, 23
- Uemura, M., Kawabata, K. S., Sasada, M., Ikejiri, Y., Sakimoto, K., Itoh, R., Yamanaka, M., Ohsugi, T., Sato, S., & Kino, M. 2010, *PASJ*, 62, 69
- Watanabe, M., Nakaya, H., Yamamuro, T., Zenno, T., Ishii, M., Okada, M., Yamazaki, A., Yamanaka, Y., et al. 2005, *PASP*, 117, 870
- Wills, D., Wills, B. J., Breger, M., & Hsu, J.-C. 1980, *AJ*, 85, 1555
- Zhang, H., Deng, W., Li, H., & Böttcher, M. 2016, *ApJ*, 817, 63